Thermal Aging of Heterophasic Propylene−Ethylene Copolymers: Spatial and Temporal Aspects of Degradation Based on ESR, ESR Imaging, and FTIR

Krzysztof Kruczala,† Jayesh G. Bokria, and Shulamith Schlick*

Department of Chemistry, University of Detroit Mercy, Detroit, Michigan 48219

Received September 30, 2002; Revised Manuscript Received January 10, 2003

ABSTRACT: Heterophasic propylene−ethylene copolymers (HPEC) containing bis(2,2,6,6-tetramethyl-4-piperidinyl) sebacate (Tinuvin 770) as a hindered amine stabilizer (HAS) were thermally aged at 393 and 433 K. Two types of HPEC were examined, containing 25 and 10% ethylene (E), respectively, as ethylene/propylene rubber (EPR). Spatial and temporal effects of the aging process were studied by electron spin resonance (ESR) and ESR imaging (ESRI) of HAS-derived nitroxide radicals and FTIR of films prepared by compression molding. The spatial distribution of the HAS-derived nitroxide radicals was obtained by 1D ESRI. These experiments enabled the visualization of an outer region of thickness ≈100 μm that contained a lower amount of nitroxides and believed to arise from the loss of the stabilizer by diffusion ("blooming") and in chemical reactions during aging. Nondestructive ("virtual") slicing of the 2D spectral spatial ESR images resulted in a series of ESR spectra that indicated the presence of nitroxide radicals in two amorphous sites, fast and slow; the corresponding relative intensity varied with sample depth. 1D and 2D ESRI allowed the detection of faster degradation of EPR in the amorphous phase represented by the fast spectral component. Both ESRI and FTIR experiments suggested a faster degradation rate in HPEC containing 25% E compared to 10% E; moreover, a larger Tinuvin 770 content in the polymers led to *less* efficient stabilization. FTIR spectra indicated increased ordering of polypropylene segments in HPEC during aging at 433 K.

Introduction

The photodegradation and thermal degradation of poly(acrylonitrile−butadiene−styrene) (ABS) containing Tinuvin 770 as the hindered amine stabilizer (HAS) (Chart 1) have been studied in our laboratory by 1D and 2D electron spin resonance imaging (ESRI).[1] This approach was based on the formation of nitroxides from the HAS during aging. Analysis of the spatial variation of ESR spectra from the HAS-derived nitroxides (HAS−NO) as a function of treatment type and duration, determined nondestructively by ESRI, provided the link to the degradation process. A major advantage of this method was the ability to track degradation processes in distinct morphological domains via the fast (F) and slow (S) spectral components detected in the ESR spectra. These two components differed in their dynamics and were assigned to nitroxide radicals located in low-T_g domains rich in butadiene (B) and in high-T_g domains rich in styrene/acrylonitrile (SAN), respectively. Results from ESRI experiments were supported by spin probe ESR experiments[2] and attenuated total reflectance Fourier transform infrared (ATR−FTIR) profiling of 50 μm thick microtomed slices.[3]

We present a study of thermal degradation in heterophasic propylene−ethylene copolymers (HPEC), which are known commercially as impact polypropylene copolymers (IPC)[4] and consist of polypropylene (PP) modified by an elastomeric component, typically ethylene−propylene rubber (EPR).[5] Morphologically, HPEC systems are more complex compared to ABS because of the presence of amorphous *and* crystalline domains. Various methods, including FTIR, differential scanning calorimetry (DSC), wide-angle X-ray scattering (WAXS), and nuclear magnetic resonance (NMR), have demonstrated the presence of *four* phases in HPEC: crystalline PP, amorphous PP, crystalline EPR (predominantly polyethylene, PE), and amorphous EPR.[6−11]

Chart 1. Hindered Amine Stabilizer (HAS) Tinuvin 770

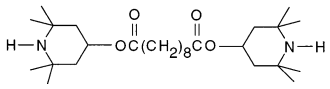

In a previous paper, referred to here as **1**,[12] we have presented a study of the HPEC morphology based on ESR spectra of HAS−NO in thermally treated HPEC samples and on comparison with the spectra of nitroxide radicals ("spin probes") doped in HPEC and in the corresponding homopolymers PP and PE. As in ABS, ESR spectra of HAS−NO and of the spin probes in HPEC were a superposition of F and S spectral components. The temperature variation of the ESR spectra has shown that both components are located in the amorphous domains of HPEC; moreover, changes in the degree of crystalline ordering due to microtoming led to changes in the relative intensities of the F and S components. The results were interpreted in terms of an additional phase, the rigid amorphous phase, whose extent and dynamics are reflected in the ESR spectra of the nitroxides. Additional support for this interpretation has been obtained by DSC and FTIR measurements.[12] The focus on morphological changes has resulted in an added benefit: it was demonstrated for the first time that ESR spectra reflect the exceptional sensitivity of nitroxide probes to polymer morphology.

In this paper we describe 1D and 2D spectral−spatial ESRI and FTIR studies of thermal aging in HPEC. The major objectives were to examine thermal degradation

† On leave from the Faculty of Chemistry, Jagiellonian University, Cracow, Poland.

* Corresponding author. E-mail schlicks@udmercy.edu.

10.1021/ma025701q CCC: $25.00
Published on Web 02/22/2003

at various temperatures, to assess the effect of ethylene content (as EPR) on the extent of degradation, and to evaluate the extent of stabilization by HAS. Results of this study will be compared to other studies of degradation in HPEC and related systems.[13−15] In terms of ESRI methodology, we introduce in this paper for the first time the automatic fit of the 1D radical profile by analytical functions using the genetic algorithm.[16]

Experimental Section

Materials. Two HPEC samples differing in their ethylene (E) content were from Dow Chemical Co.: HPEC1 (IPC, C 708, M_n = 60 700, M_w = 227 000) and HPEC2 (IPC, C104-01, M_n = 90 400, M_w = 428 000). The E content in the HPEC samples, determined as described in part 1, was 25 wt % in HPEC1 and 10 wt % in HPEC2, within ±2%.

Preparation of Samples for ESR and ESRI. HPEC samples containing 1 and 2 wt % Tinuvin 770, as plaques prepared by injection molding, were aged in a convection oven at 393 and 433 K. For the ESR experiments, cylindrical samples with diameter ≈7 mm were cut from the plaques at selected time intervals, trimmed to fit the 5 mm in diameter of the ESR sample tube, and placed in the ESR resonator with the symmetry axis along the long axis of the resonator and parallel to the direction of the magnetic field gradient. The ESR spectra of HAS−NO were measured in the temperature range 100−433 K as a function of treatment time at a given temperature. The sample notation is HPEC-*n*H, where *n* indicates wt % HAS. All the results presented in the next section are for HPEC-1H, unless indicated otherwise.

ESR Measurements. Spectra were collected with Bruker X-band EMX spectrometers operating at 9.7 GHz with 100 kHz magnetic field modulation and equipped with the Acquisit 32 Bit WINEPR data system version 3.01 for acquisition and manipulation and the ER 4111 VT variable temperature units. The microwave frequency was measured with a Hewlett-Packard 5350B microwave frequency counter. Most spectra were measured with the following parameters: sweep width 120 G, microwave power 2 mW, time constant 40.96 ms, conversion time 81.92 ms, 4−10 scans, and 1024−2048 points. The modulation amplitude was varied in the range 0.5−1.2 G, depending on line width. The temperature was controlled within ±1 K. All samples were allowed to equilibrate for at least 10 min after reaching the desired temperature. Additional experimental details, including the determination of HAS−NO concentration in whole samples and of the relative intensity of the F and S components, have been described.[1,2,12]

ESR Imaging and Data Acquisition. One of the ESR spectrometers was equipped with two Lewis coils and two regulated dc power supplies for the imaging experiments. The intensity profile of radicals was deduced from 1D ESRI experiments. Two spectra are needed: the regular ESR spectrum and the spectrum measured in the presence of the magnetic field gradient ("1D image"). The 1D image is a convolution of the ESR spectrum in the absence of the gradient with the distribution of the paramagnetic centers along the gradient direction ("the profile"). The convolution is correct if the ESR line shape has no spatial dependence. The two spectra needed were measured at 240 K in order to "freeze" the fast component or at 340 K in order to reach the motional narrowing regime of both spectral components; in this way the spatial dependence of the ESR signal was avoided.[1a] The 1D images were obtained with a field gradient of 206 G/cm unless otherwise indicated.

In our initial ESRI studies the concentration profiles of the radicals were deduced by Fourier transform followed by optimization with the Monte Carlo (MC) procedure.[1a,c,17] The disadvantage of this method is the high-frequency noise present in the optimized profiles. In our most recent publications, the intensity profile was fitted by analytical functions and convoluted with the ESR spectrum measured in the absence of the field gradient in order to simulate the 1D image.[1d,e] The best fit was obtained by variation of the analytical function (Gauss or Boltzmann, for example) and of the numerical parameters of the chosen function in order to obtain good agreement with the 1D image; the best fit was selected by visual inspection.

We present the implementation of the genetic algorithm[18] for minimization of the difference between simulated and experimental 1D images; this procedure allows the best fit to be chosen automatically. Details will be described in a future publication,[16] and only a brief description will be given here. A typical genetic algorithm (GA) consists of the following basic operations: creation of the initial population, calculation of the fit to experimental data, selection of the couples, reproduction, and mutation.[18] The terminology is adopted from biology. The ability of the GA to obtain a global minimum energy has been demonstrated and discussed.[19]

In the first step the GA implemented in our laboratory calculates an initial population of *N* profiles (typically 100) by random selection of the parameters for the chosen analytical functions. The profiles are then convoluted with the experimental spectrum, and the results are ranked according to the fit to the experimental 1D image. The next steps are selection of the "parents", reproduction (including crossover), and mutation. Mutation introduces changes in a small number of randomly chosen parameters. The program accommodates two operators for mutation; one operator allows variation in a given range of a certain number of parameters (typically 5%); the second operator replaces a smaller number of parameters, 10% of the number of parameters modified by the previous operator, by random numbers. After the new population is selected, the entire process is repeated until the fit to experimental data is considered satisfactory.[19−21] The GA was implemented on a PC run by the Windows XP operating system and equipped with a Pentium 4 1.7 GHz processor. In the case of the profile presented in Figure 1, the root-mean-square (rms) values were 23.2 for 200 iterations (1 min), 16.6 for 2000 iterations (12 min), 16.1 for 5000 iterations (28 min), and 15.8 for 20 000 iterations (<2 h). In most cases the difference between 5000 and 20 000 iterations was not visually detectable in the residual to the fit. Typical root-mean-square (rms) values were 13 for MC and 16 for GA methods. The simulation times and the corresponding rms values may change because the initial set of parameters is selected by the algorithm in a random fashion.

Figure 1 compares the results obtained by MC optimization (A) and by the GA (B) for the determination of the 1D profile; the sample was HAS−NO in HPEC2-1H treated at 433 K for 7 days. The experimental 1D images, the simulated 1D images (deduced by convoluting the profile shown in Figure 1A with the ESR spectrum measured in the absence of the gradient), and the residual of the fits are also shown in (A) and (B). The concentration profile deduced by the GA (Figure 1B) was simulated by 10 Gaussian functions convoluted with two Boltzmann functions; the latter appeared at the edges of the profiles and improved the fit to the 1D image. The selection of these analytical functions is based on our extensive previous experience with various types of functions and with variations of the corresponding parameters.[1d,c] The agreement between experimental and simulated 1D images is very good, but not as good as for the MC procedure, which calculates the 1D image point-by-point. The advantage in the case of the simulation by analytical functions is the absence of noise in the profile, which allows the detection of details that would be lost when using the MC procedure (vide infra; Figures 5 and 6). All 1D profiles shown below were deduced using the same combination of analytical functions.

To obtain the most accurate details in the 1D profiles, the sensitivity profile of the ESR resonator was determined. To this end, an HPEC2-2H plaque was thermally treated for 168 days at 393 K. Then the rod at the top of the plaque was cut, and a cylindrical piece ≈4 mm in diameter and 5.65 mm long was selected for analysis, as shown in Figure 2A,B. The profile of HAS−NO radicals was then deduced from ESR spectra measured at 340 K (Figure 2C, red). No heterogeneity in radical distribution along the axis of the cylinder was expected

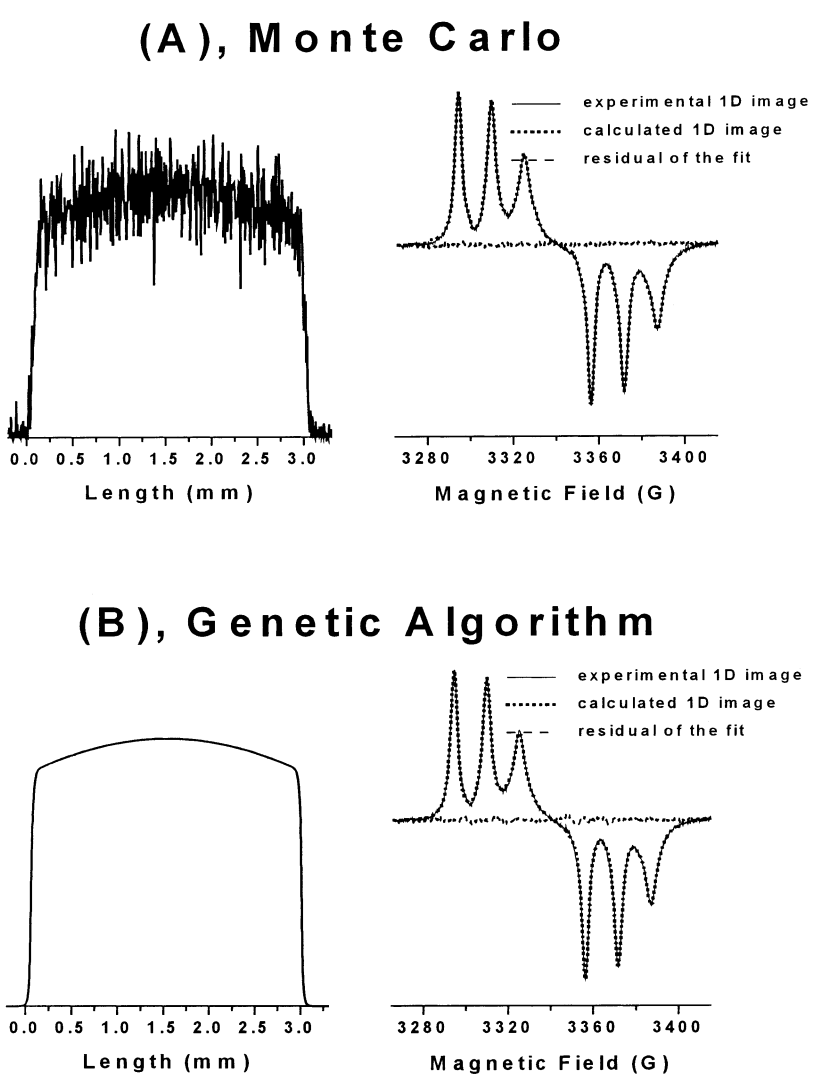

Figure 1. 1D images and concentration profiles of HAS−NO in HPEC2 treated at 433 K for 7 days: (A, left) profile obtained by Monte Carlo optimization; (B, left) optimized profile calculated by the genetic algorithm, with 10 Gaussian lines for the central part and convoluted at the edges with Boltzmann functions. The 1D images measured at 340 K and gradient of 206 G/cm, the calculated 1D images, and the residual of the fits are shown on the right side in (A) and (B). The residual of the fit in (B) is shown for the genetic algorithm after 20 000 iterations. See text.

since the entire rod length was equally exposed to oxygen and heat. To prove this assumption, the nitroxide profile in a 3.20 mm long cylinder cut from the longer cylinder was also determined. As seen in Figure 2C, the profiles of the two cylinders are identical in the overlap region, thus confirming the original assumption. The sensitivity profile was used to correct all the profiles presented below for samples cut into the depth of the plaques.

The 2D spectral−spatial ESR images were reconstructed from a complete set of projections, typically 128, collected as a function of the magnetic field gradient, using a convoluted back-projection algorithm.[1b−e] In the first reconstruction stage, the projections at the missing angles were assumed to be identical to the projection measured at the largest available angle. In the second stage, the projections at the missing angles were obtained by the projection slice algorithm (PSA)[22,23] with 2−10 iterations. The 2D image is saved as a 256 × 256 matrix.

FTIR Measurements. Films of HPEC containing 0 and 1% HAS were obtained respectively from neat polymer pellets and from plaques prepared by injection molding. The polymer was placed on aluminum foil and compression-molded between two preheated flat molds in a Carver press for 30 s at ≈475 K and a pressure of 1600 atm. The films were suspended inside a convection oven and thermally treated at 433 K. FTIR spectra were acquired at selected time intervals; Table 1 lists the treatment time for the films prepared for FTIR measurements. At least two films for each sample were analyzed. Upon thermal treatment, all films became increasingly brittle. HPEC1-0H and HPEC1-1H samples became charred. The effect was pronounced in HPEC1-1H after only 39 h of treatment; after 63 h of treatment the films disintegrated, and it was not possible to measure their FTIR spectra. In the case of HPEC1-0H, HPEC2-0H, and HPEC2-1H, the films disintegrated after approximately 88, 136, and 113 h, respectively. For the same time of thermal treatment, HPEC2 films were visually less affected compared to HPEC1 films. FTIR spectra were also measured for several remolded films of HPEC2-1H, prepared from films treated at 433 K for 100 h. Major differences were evident in the physical appearance of the treated films before and after compression molding. When

Table 1. Treatment Times of Films Measured by FTIR

	treatment time (in h) at 433 K					
sample	0	39	63	88	113	136
HPEC1-0H	√	√	√	√[a]	−	−
HPEC1-1H	√	√[a]	−	−	−	−
HPEC2-0H	√	√	√	√	√	√
HPEC2-1H	√	√	√	√	√[a]	−

[a] At this stage the films disintegrated and treatment could not be continued.

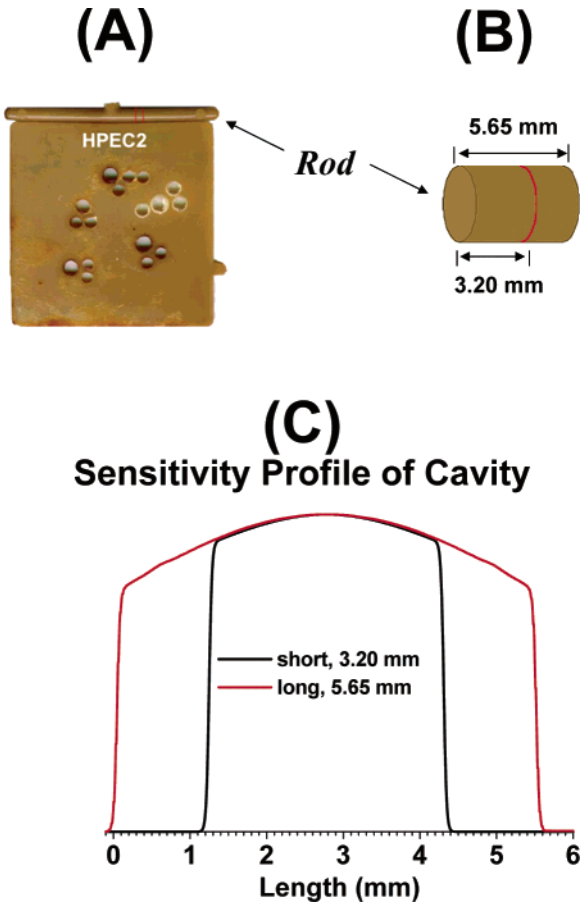

Figure 2. Sensitivity profile of the resonator: (A) HPEC2-2H plaque treated at 393 K for 168 days. The part between the two red lines was analyzed; the total length was 5.65 mm. (B) Cylindrical top of the plaque used for 1D ESRI experiments. The part to the left of the red border was 3.2 mm. (C) Nitroxide profile of the short (black) and long (red) cylinders. See text.

removed from the oven, the films were fragile and shattered easily; after remolding, however, plasticity was restored.

FTIR spectra of the films were acquired in the transmission mode using the Perkin-Elmer Spectrum 2000 FTIR spectrometer equipped with a mid-IR (MIR) globar source and a triglycine sulfate (TGS) detector. During acquisition the film was held in place with a magnetic film holder.

Spectra were measured in the range 4000−400 cm^{-1} with 4 cm^{-1} resolution and eight scans; each scan was automatically corrected for open-beam background. The C=O ester stretch of Tinuvin 770 was detected in the FTIR spectra of HPEC1-1H and HPEC2-1H at 1737 cm^{-1}. This assignment was confirmed by comparing spectra for samples containing 0 and 2 wt % HAS. We note that the carbonyl peak from the HAS appeared at 1728 cm^{-1} in ABS (determined by ATR−FTIR)[3] and at 1722 cm^{-1} in a chloroform solution of HAS.

Results

ESR Spectra of HAS−NO in HPEC1 and HPEC2. In Figure 3 we present ESR spectra in the temperature range 100−433 K for HAS−NO in HPEC1-1H and HPEC2-1H thermally treated at 433 K for 10 days. The rigid limit spectrum at 100 K changed as the temperature increased, and at 300 K both fast and slow components appeared. The line shapes at 340 K are typical for rotation of the probe along the long axis of HAS−NO and can be simulated with a diffusion tilt angle, ϑ, equal to 90°.[1a] The angle ϑ is between the direction of the N−O bond and the axis of the 2p orbital

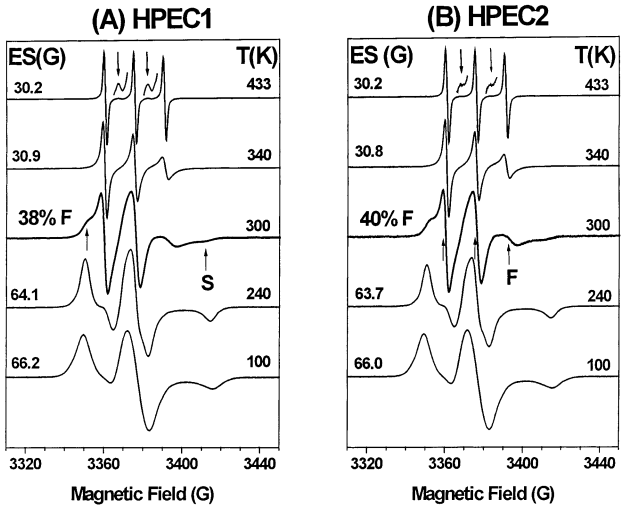

Figure 3. ESR spectra for HAS−NO in HPEC1 (A) and HPEC2 (B) thermally treated at 433 K for 10 days. The % F at 300 K is indicated in (A) and (B). Downward arrows next to vertically expanded portions of the spectra measured at 433 K point to signals from the biradical nitroxide species 2NO−HAS. Upward arrows point to the S and F spectral components.

of the unpaired electron. As discussed in **1**,[12] the nitroxide radicals reflect the dynamics in the amorphous domains. The relative intensities of the two spectral components at 300 K in the HPEC samples were deduced by deconvolution, as described;[1] at 300 K, % F = 38 in HPEC1 and 40 in HPEC2. The vertically expanded portions of the spectra measured at 433 K (downward arrows in Figure 3) indicate signals from the biradical, 2NO−HAS, in both samples. These signals are more intense in HPEC1, even though the nitroxide concentration is slightly lower compared to HPEC2 (Figure 4B, described below). We assign this effect to the larger E content (as EPR) in HPEC1, which leads to lower microviscosity.

The concentration of HAS−NO in HPEC1 and HPEC2 (whole samples) as a function of treatment time, t, is presented in parts A and B of Figure 4 for treatment at 393 and 433 K, respectively. For treatment at 393 K, the radical concentration increases with t and is lower for t < 110 h and higher for $t \geq 110$ h in HPEC2 compared to HPEC1. This "crossover" in nitroxide concentration can be explained by the higher consumption of the stabilizer in HPEC1 due to the higher content of the more degradable EPR component (vide infra). For treatment at 433 K, the radical concentration reaches a maximum in HPEC2 and then decreases; the HPEC1 sample shattered for t >10 days, and it was not possible to measure the radical intensity. The crossover in radical concentration for the two polymers is also seen for samples treated at 433 K, but after shorter treatment times, ≈5 days (Figure 4B).

The corresponding relative intensity of the F component, % F, is shown in Figure 4C,D. Two important conclusions can be deduced from the variation of % F in the two samples with treatment temperature and time. First, the F content in samples treated at 393 K is fairly constant: 35−37% in HPEC2 and 41−43% in HPEC1 (Figure 4C). For treatment at 433 K, however, % F reaches a maximum and then decreases as the time of treatment increases; the significant rate of decrease for % F in HPEC1 compared to HPEC2 emphasizes the consumption of the stabilizer in the sample that con-

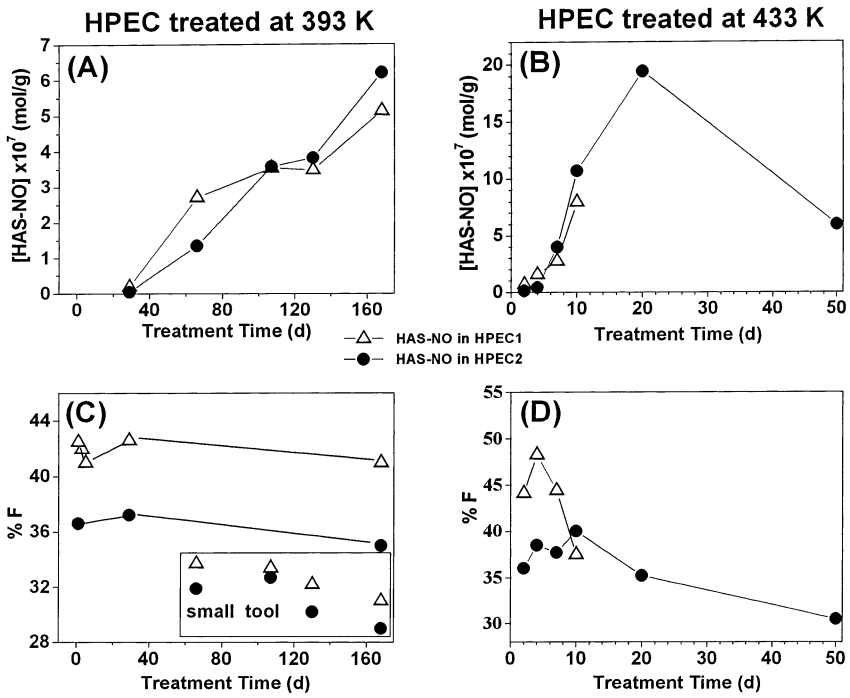

Figure 4. Concentration of HAS−NO and % F in the ESR spectra at 300 K as a function of thermal treatment for HPEC1 (△) and HPEC2 (●): (A) HAS−NO for thermal treatment at 393 K; (B) HAS−NO for thermal treatment at 433 K; (C) % F for thermal treatment at 393 K; (D) % F for thermal treatment at 433 K.

tains a larger EPR content. We note that according to data presented in part 1, HPEC1 contains 41 wt % EPR, and 26 wt % EPR is represented by the F component; HPEC2 contains 31 wt % EPR, and 21 wt % EPR is represented by the F component; these values were deduced from spectra measured at 300 K. Second, we notice the lower % F in both samples when the samples were cut with a tool of a smaller diameter (Figure 3C, framed inset); this result was explained in part 1 by the formation of a larger amount of the rigid amorphous phase in samples exposed to stress, which leads to additional ordering.

1D and 2D Spectral−Spatial ESRI. Concentration profiles of HAS−NO in HPEC1 and HPEC2 for the same treatment times, 29 and 168 days, at 393 K are presented in Figure 5. All profiles were corrected for the sensitivity profiles of the resonator as described in the Experimental Section; for ease of comparison, the resonator profile measured for the longer cylindrical sample (5.65 mm) in the region of interest is also shown in Figure 5A together with the uncorrected profile. The 1D profiles show the formation of an outside layer that contains a lower amount of nitroxide radicals. The layer is more pronounced for HPEC1: in this sample the effect is seen already after 29 days of treatment. For the same time of treatment the outside layer in HPEC2 is not as visible but becomes more pronounced after 168 days of treatment.

The nitroxide-depleted region is not detected in the 1D profiles of HAS−NO in HPEC1 samples treated at 433 K for 4 and 7 days (Figure 6A) and in HPEC2 samples treated for 7, 10, and 50 days (Figure 6B). After 10 days of treatment at 433 K, the diffusion-limited oxidation (DLO) regime[24] is clearly observed for HPEC1.

2D spectral−spatial ESRI perspective plots at 300 K and corresponding spectral slices in the derivative mode are shown for HAS−NO in HPEC1 treated at 393 K for 168 days (Figure 7A) and at 433 K for 10 days (Figure 7A). Comparison of the spectral slices in Figure 7A,B

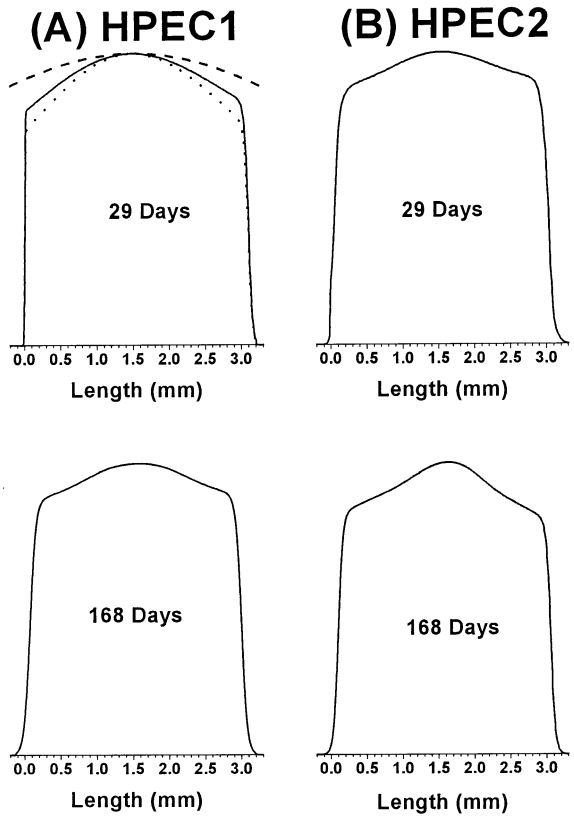

Figure 5. Concentration profiles of HAS−NO deduced from 1D ESRI experiments for the indicated treatment times in days at 393 K: (A) HPEC1 (29 and 168 days); (B) HPEC2 (29 and 168 days). For HPEC1 treated for 29 days, the corrected profile (black) is shown together with the sensitivity profile of the resonator (red) and the uncorrected profile (green).

indicates a lower % F in Figure 7B throughout the sample depth. This result, combined with the DLO regime evidenced in the perspective plot, indicates more advanced degradation for the sample treated at the

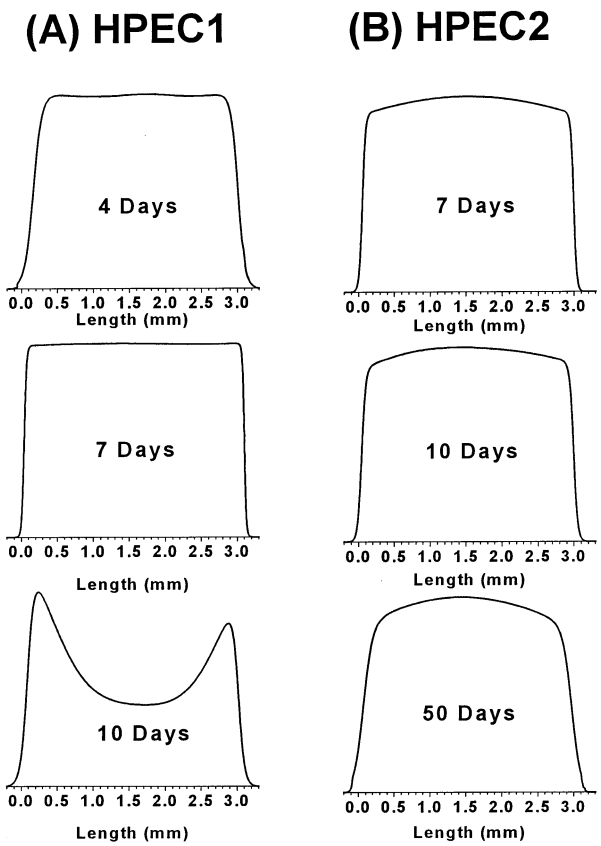

Figure 6. Concentration profiles of HAS−NO deduced from 1D ESRI experiments for the indicated treatment times in days at 433 K: (A) HPEC1 (4, 7, 10 days); (B) HPEC2 (7, 10, 50 days).

higher temperature, even though the treatment time was much shorter, 10 vs 168 days.

In Figure 8 we present spectral profiling: the variation of % F at 300 K in the plaques as a function of sample depth in HPEC1 and HPEC2 treated at 393 and 433 K. The most significant result is the formation of a narrow skin, ≈100 μm thick, that contains a lower % F at both treatment temperatures (Figure 8A−D).

Snapshots of HPEC plaques containing 1 and 2% HAS and treated at 433 K for 10 days are shown in Figure 9. It is clearly seen that HPEC2 samples are more homogeneously colored compared to HPEC1. Moreover, in HPEC1 additional discoloration is seen near the edges and missing parts (where samples were cut), most likely due to the availability of more oxygen; this effect is more pronounced for HPEC1-2H compared to HPEC1-1H. Visual inspection of the plaques provided a guide for the choice of location for the samples to be cut: in the more homogeneously colored regions.

FTIR Measurements. All FTIR spectra were normalized to the CH_3 symmetric bend (umbrella) peak at 1377 cm^{-1}. Spectra in the carbonyl region for HPEC1-0H and HPEC2-0H for selected treatment times at 433 K are shown in Figure 10. We notice the appearance of the carbonyl peak after shorter treatment times for HPEC1 (88 h) compared to HPEC2 (136 h).

In Figure 11 we present the carbonyl region for HPEC2-0H and HPEC2-1H for the indicated treatment times at 433 K. The carbonyl peak appears in the neat polymer for t = 136 h (Figure 11A), and at shorter t, 113 h, in the HAS-stabilized polymer (Figure 11B). The disappearance of the carbonyl peak from HAS after $t \geq$ 5 h is clearly seen for HPEC1-1H (Figure 11B). Samples in which the HAS disappeared also showed a negligible ESR signal from HAS−NO.

Changes in morphology of the HPEC samples during thermal treatment are shown in Figure 12. The regularity peaks at 998 and 973 cm^{-1} are presented for HPEC2-1H as a function of treatment time. The regularity ratio (RR), the ratio of signals at 998 and 973 cm^{-1}, $A(998)/A(973)$, is plotted in the inset as a function of treatment time; the increase of RR is an indicator of higher degree of crystallinity.[9] When samples treated for 100 h at 433 K were remolded, the regularity index is back to the value of ≈0.8 measured before thermal treatment (see arrow in the inset of Figure 12).

Discussion

In this section we will discuss the degradation in HPEC as a function of EPR content; the behavior of, and the extent of stabilization by, the HAS during thermal treatment; and morphological effects in HPEC during thermal treatment.

Degradation of HPEC as a Function of EPR Content. Conclusions on this topic will be drawn from the variation of the nitroxide content and % F in whole samples vs treatment time and temperature (Figure 4), the radical profiles within sample depth (Figures 5 and 6), snapshots of HPEC1 and HPEC2 plaques during thermal aging (Figure 9), and FTIR spectra of HPEC1-0H and HPEC2-0H in the carbonyl region (Figure 10).

Figure 4A indicates that for treatment at 393 K the concentration of HAS−NO in whole samples is higher in HPEC1 for $t \leq$ 110 days, and lower for $t >$ 110 h, compared to HPEC2. The higher nitroxide content in HPEC1 in the early stages of thermal treatment can be explained by the expected higher diffusion of oxygen, HAS, and HAS−NO in samples containing a larger amount of E (as EPR). The diffusion coefficient, D, of Tinuvin 770 in PP is 2.7×10^{-10} cm^2/s in the temperature range 298−348 K and much higher in PE (74×10^{-10} cm^2/s) in a similar temperature range (328−353 K).[25,26] The lower nitroxide content in HPEC1 as the treatment time increases cannot be explained if the only difference between the two HPEC samples is the rate of diffusion of oxygen and the mobility of other reactants. The explanation we offer is a higher consumption of nitroxides due to higher degradation rate in HPEC1 compared to HPEC2. This idea is reinforced by data in Figure 4D, which show that the disappearance of the fast component for treatment at 433 K is much faster for HPEC1 than for HPEC2. We recall that the F component represents radicals located in unrestrained (by crystallites) EPR domains.

The concentration profiles shown in Figures 5 and 6 provide additional evidence for this interpretation. The DLO regime is clearly reached for HPEC1 after 10 days of treatment at 433 K (bottom profile in Figure 6A), indicating the advanced stage of oxidation; for HPEC2, the 1D profiles are almost flat even after 50 days of treatment at the same temperature (Figure 6B). The faster degradation in HPEC1 is also seen by comparing the appearance of similarly treated HPEC samples containing 1 and 2 wt % HAS (Figure 9).

Further evidence is seen in the carbonyl region of FTIR spectra for HPEC1-0H and HPEC2-0H treated at 433 K (Figure 10): The formation of carbonyls in HPEC1 is detected after a shorter treatment time (88 h) compared to HPEC2 (136 h).

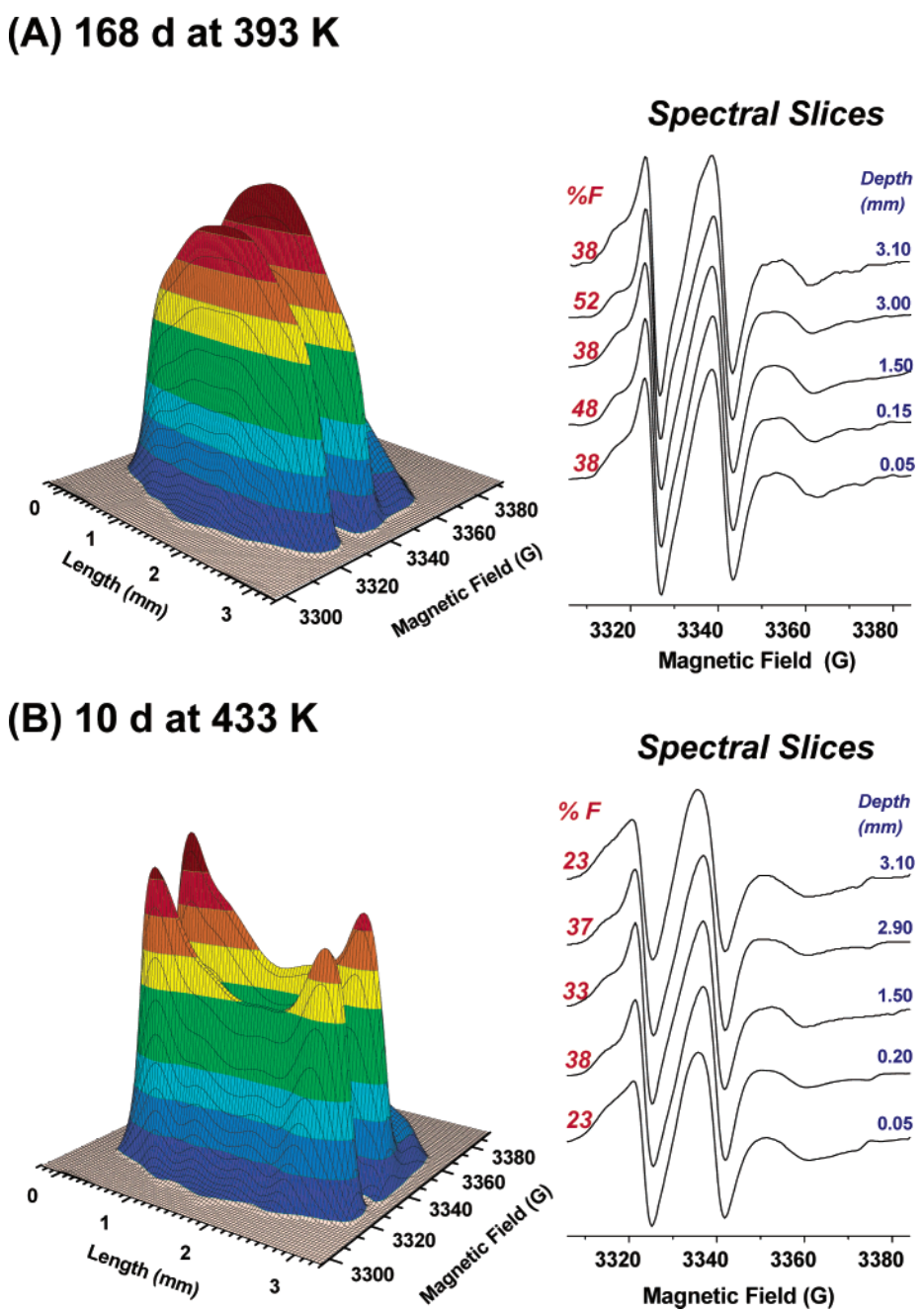

Figure 7. 2D spectral−spatial ESRI perspective images at 300 K and corresponding spectral slices for HAS−NO in HPEC1: (A) treated at 393 K for 168 days; (B) treated at 433 K for 10 days.

In a study of photooxidation and thermal (at 423 K) oxidation of HPEC containing 15% E (as EPR), it was suggested that the major degraded component is PP. This conclusion was based on FTIR spectra and analysis of volatile degradation products. The results were interpreted in terms of a degradation cascade based on oxidation initiated at the tertiary carbon in the propylene repeat unit.[13] The mechanical properties of HPEC (termed "impact-modified iPP") thermally treated at 393 K were also investigated; the sample contained 15% EPR, and the results were considered together with, and similar to, the results for PP.[14] It is no surprise that in samples containing ≥85% P the degradation process is driven by this repeat unit.[13,14]

To the best of our knowledge no investigation of the composition dependence of degradation in HPEC has been published. The variation of the E content presented in this study emphasized that the EPR component is an important factor in degradation. The initial point of attack may still be the tertiary carbon in propylene. The data presented here indicate however that the rate of aging processes in HPEC is determined by the increased rate of oxygen diffusion and reactants mobility in polymers with higher EPR content. The higher proportion of the amorphous domains in HPEC1 compared to HPEC2, 63 vs 60%, and the corresponding higher amount of the EPR represented by the F component, 26 vs 21,[12] may also enhance the local reactivity. The presence of stronger signals for 2HAS−NO in HPEC1 in the ESR spectra measured at 433 K (Figure 3) is evidence for the higher mobility in this system compared to HPEC2.

Behavior of HAS during Thermal Treatment. The 1D profiles shown in Figure 5 for HPEC samples

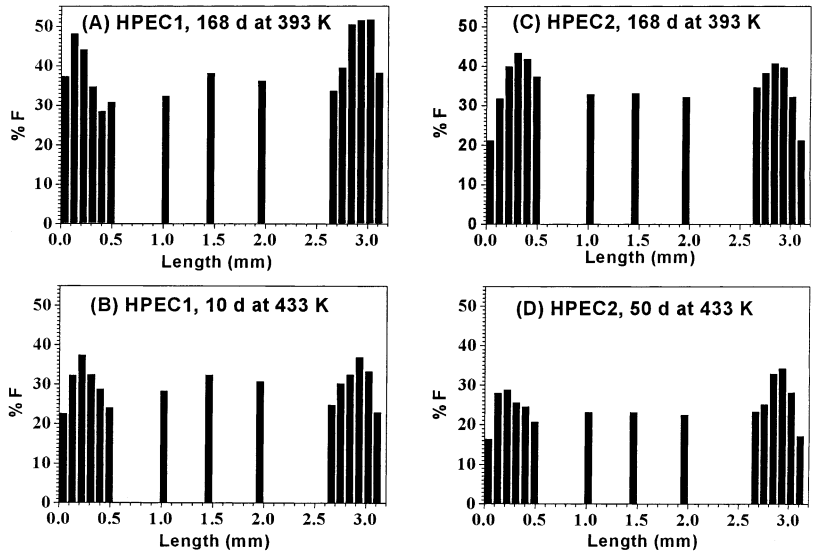

Figure 8. Spectral profiling: Variation of % F with sample depth for HAS−NO in HPEC1 treated for 168 days at 393 K (A) and for 10 days at 433 K (B) and in HPEC2 treated for 168 days at 393 K (C) and for 50 days at 433 K (D). The data were deduced from 100 μm thick virtual (nondestructive) slices in the corresponding 2D spectral−spatial ESR images.

treated at 393 K indicate less nitroxides in the outer regions of the plaques; the effect is seen even after only 29 days of treatment. At 393 K the degradation process is very slow, as clearly seen by the absence of carbonyl peaks in the FTIR data (data not shown) and in Figure 3A,C, which show increasing HAS−NO and steady % F for both polymers with time of treatment; therefore, no serious complications due to consumption of HAS as stabilizer are expected. We suggest that the outer layer depleted in nitroxide radicals is due to the loss of HAS; the loss is initially more pronounced in HPEC1 because of the higher E content, which increases the mobility of the additive. In HPEC2 treated at 393 K the effect becomes pronounced after longer treatment times (bottom profile in Figure 5B, t = 168 days), most likely because the diffusion of the additive is slower in this system, which contains less E. The higher nitroxide content in the plaque center is also seen in the 2D spectral−spatial ESRI perspective plot shown in Figure 7A for HPEC1 treated at 393 K.

For treatment at 433 K the loss of additive and the formation and consumption of nitroxides are enhanced; the balance of these processes is the most reasonable cause for the essentially flat profiles seen in Figure 6, with the exception of HPEC1 after 10 days of treatment (lower profile in Figure 6A). The DLO regime reached in HPEC1, also seen in 2D ESRI experiments (Figure 7B), clearly shows the formation of more HAS−NO at the sample extremities due to access to oxygen.

Spectral profiling data are shown in Figure 8 for HPEC1 and HPEC2 as a function of time and temperature of thermal treatment. In all profiles we notice an outer slice, ≈100 μm thick, depleted in the F component. The effect is detected for both HPEC samples for treatment at 393 and 433 K. The lower % F can be due to the loss of the stabilizer in the outer region, as also seen in the loss of HAS−NO in the 1D profiles, and also to consumption of nitroxides in specific morphological domains (see below). The loss of the additive during thermal treatment ("blooming") is directly seen in the FTIR spectra of HPEC2-1H films (Figure 11B): the carbonyl peak from the HAS disappears after 5 h of treatment at 433 K.

The effect of HAS on the degradation process can be assessed by comparing FTIR spectra in the carbonyl region for HPEC2-0H and HPEC2-1H films (Figure 11A,B): The spectra suggest more extensive degradation in HPEC2-1H, judging by the time necessary to detect the carbonyl peak: 136 h in HPEC2-0H and only 113 h in HPEC2-1H. In parallel, HAS−NO is not detected in the ESR spectra after 5 h of treatment. We tentatively suggest that fragments from HAS are reactive and lead to degradation. This idea is confirmed by the snapshots of plaques, which show more discoloration in samples containing 2% HAS (Figure 9) for polymers treated at 433 K. Evidence for reaction products of HAS with HPEC has been presented;[13] some of these products may promote degradation.

The antiprotective effect of HAS has also been detected in the thermal degradation of ABS polymers at 353 and 393 K.[1d,e] For iPP, results have indicated that the HAS is a more efficient stabilizer at lower temperatures.[14] Of course, the range of "high" or "low" temperatures depends on the particular systems and must be investigated and defined for each case.

Morphological Effects during Thermal Treatment. The spectral slices deduced from 2D ESRI experiments and shown in Figure 7, as well as spectral profiling (Figure 8), indicate that the % F is lower in the center of the plaques; the effect is small but consistent in all samples, even for the plaque that exhibits the DLO regime (Figure 7B). We note that the lower % F is seen in plaque regions that clearly show a higher total nitroxide content in the 1D profiles (Figures 5 and 6). This effect can be rationalized by the assumption that the F component, which reflects nitroxides located in the dynamically unrestricted amorphous domains,[12] is consumed preferentially during the aging process. Support for this idea is provided by Figure 4D, which shows the significant decrease in % F for HPEC1 with treatment time; the decrease in % F is also seen in the same figure for HPEC2, but less dramatic compared to HPEC1 for the reasons outlined in the previous section. This is a significant conclusion because it emphasizes the ability of ESRI experiments to detect variations in the degree of aging in different morpho-

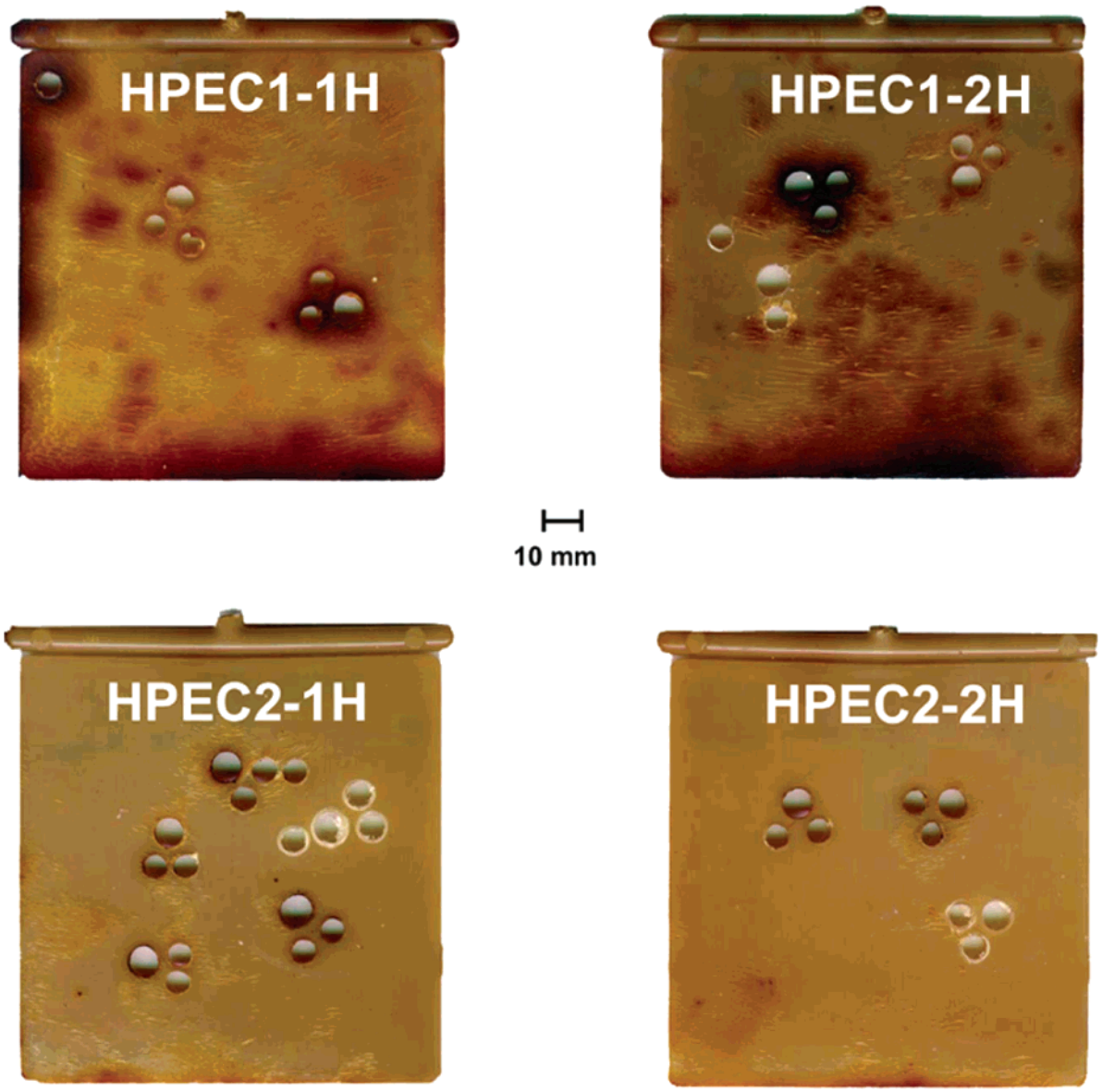

Figure 9. Snapshot of HPEC1 and HPEC2 plaques containing 1 and 2% HAS and thermally treated at 433 K for 10 days.

logical domains. In the case of ABS, this ability consisted in visualization of high- and low-T_g domains. In the case HPEC we are able to distinguish preferential aging in EPR domains represented by the F component of HAS−NO.

A second morphological effect was detected in the FTIR spectra of HPEC films: Figure 12 shows the increase of the regularity ratio, RR, in HPEC-1H films with treatment time at 433 K and therefore the increase of the degree of crystallinity in HPEC2 during aging; a similar result was obtained for HPEC1 films. These results are in agreement with known data in the literature: Crystallization in PP has been proposed as the degradation processes advance due to the formation of shorter chains that more easily rearrange into ordered domains.[14,29] To check the reversibility of the crystallization process in the HPEC samples, the RR was measured in the FTIR spectra of remolded films (Figure 12, inset). The RR was lower, 0.83, and similar to the original value for the untreated film when measured immediately after thermal treatment; moreover, the RR in the same film after 3 months was only slightly higher, 0.88. The decrease in the molecular mass of polymer chains during aging is clearly taking place. The results obtained in the present study indicate, however, that the process responsible for increase in the degree of crystallinity in PP is not only breaking of chains but also morphological changes.

In the case of samples prepared by injection molding of PP/EPR blends, depth-profiling studies have revealed the formation of a skin consisting of several layers ("stratification"), whose composition is different compared to the bulk phase;[14,30,31] the effect was explained by postprocessing temperature variations in the sample upon cooling. Similar effects have been detected earlier in PP samples and assigned to flow, shear, and temperature variations during and following processing.[32] In the case of PP/EPR blends,[30,31] a transcrystalline layer (≈10 μm thick) followed by an elastomer region (≈20 μm thick) was detected in the outer regions of injection-molded samples. The resolution in the ESRI experiment is ≈100 μm so we cannot visualize these narrow regions. It is quite possible, however, that the outer slice depleted in the F component seen in Figure 8 is due to the presence of a crystalline PP layer; if this is the case, the effect is seen in the ESRI experiments

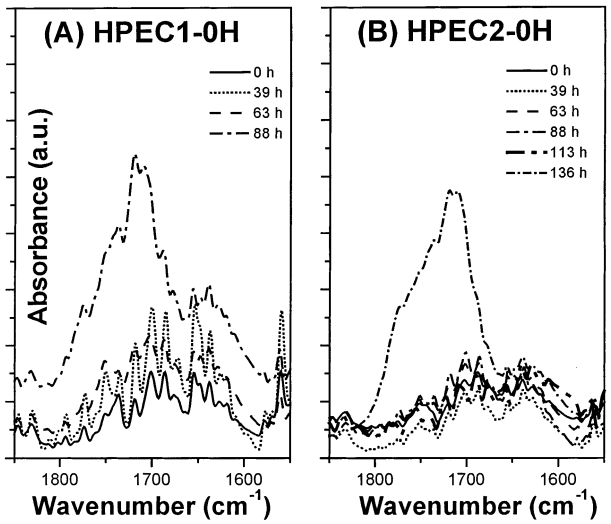

Figure 10. FTIR spectra in the carbonyl region for HPEC1-0H (A) and HPEC2-0H (B) after selected treatment times at 433 K. The spectra were normalized to the CH_3 umbrella mode at 1377 cm^{-1}.

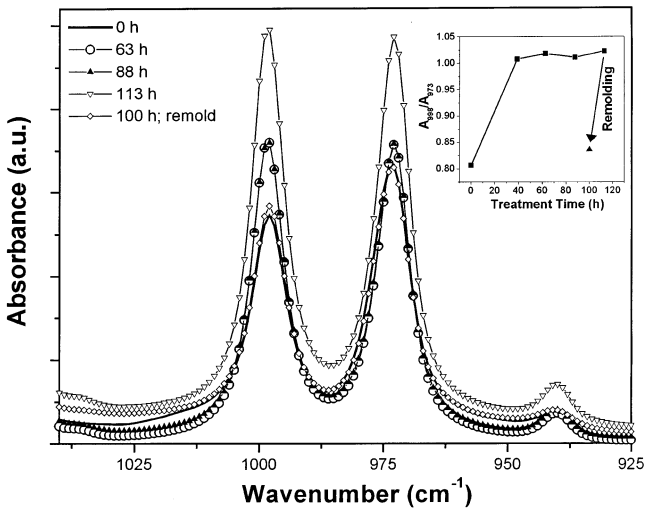

Figure 11. FTIR spectra in the carbonyl region for HPEC2-0H (A) and HPEC2-1H (B) after selected treatment times at 433 K. The spectra were normalized to the CH_3 umbrella mode at 1377 cm^{-1}. Note the disappearance of the carbonyl signal from HAS at 1737 cm^{-1} after 5 h of thermal treatment.

as part of a larger region and therefore not as pronounced as it really is.

Conclusions

Heterophasic propylene−ethylene copolymers (HPEC) containing bis(2,2,6,6-tetramethyl-4-piperidinyl) sebacate (Tinuvin 770) as a hindered amine stabilizer (HAS) were thermally aged at 393 and 433 K and studied by ESR, ESR imaging (ESRI), and FTIR. Two types of HPEC were examined, containing ≈25 and ≈10% ethylene (E), respectively, as ethylene/propylene rubber (EPR).

Both ESRI and FTIR experiments suggested a faster degradation rate in HPEC containing 25% E compared to 10% E. The spatial distribution of the HAS-derived nitroxide radicals obtained by 1D ESRI enabled the visualization of an outer region of thickness ≈100 μm that contained a lower amount of nitroxides, and believed to arise from the loss of the stabilizer during aging, by diffusion ("blooming") and by chemical reactions. Nondestructive ("virtual") slicing of the 2D spectral−spatial ESR images resulted in a series of ESR spectra, which indicated the presence of nitroxide radicals in two amorphous sites, fast and slow; the corresponding relative intensity varied with sample depth. 1D and 2D ESRI allowed the detection of faster degradation in the amorphous EPR phase represented by the fast spectral component. This study emphasized the ability of ESRI experiments to track aging in different morphological domains.

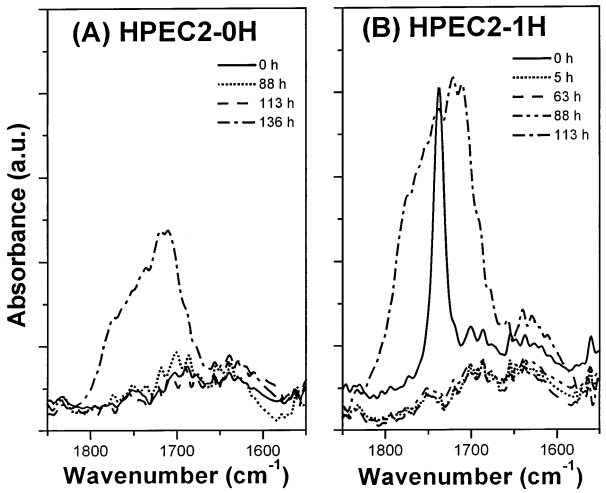

Figure 12. Variation of IR regularity peaks associated with iPP in HPEC2-1H films treated for 0, 63, 88, and 113 h at 433 K and in the sample obtained by remolding of the film treated for 100 h. The inset shows the regularity ratio, *A*(998)/*A*(973), as a function of treatment time and after remolding of the treated film.

The effect of HAS is antiprotective: the presence and a larger of Tinuvin 770 content in the polymers led to *less* efficient stabilization. FTIR spectra indicated increased regularity of polypropylene segments in HPEC during aging at 433 K. ESR spectra showed the formation of nitroxide biradicals as a result of thermal treatment at 433 K.

Acknowledgment. We are grateful to the Polymers Program of the National Science Foundation for support of this study. We thank Dow and Ciba Companies for the gift of ABS and HAS, respectively. Special thanks are due to John L. Gerlock for his ideas and suggestions, Mikhail M. Motyakin for his help with sample preparation and initial measurements, and Rose A. Ryntz (Visteon Corporation) for useful discussions on HPEC morphology.

References and Notes

(1) (a) Motyakin, M. V.; Gerlock, J. L.; Schlick, S. *Macromolecules* **1999**, *32*, 5463. (b) Kruczala, K.; Motyakin, M. V.; Schlick, S. *J. Phys. Chem. B* **2000**, *104*, 3387. (c) Motyakin, M. V.; Schlick, S. *Macromolecules* **2001**, *34*, 2854. (d) Motyakin, M. V.; Schlick, S. *Polym. Degrad. Stab.* **2002**, *76*, 25. (e) Motyakin, M. V.; Schlick, S. *Macromolecules* **2002**, *35*, 3984.

(2) Varghese, B.; Schlick, S. (a) *J. Polym. Sci., Part B: Polym. Phys.* **2002**, *40*, 415. (b) Varghese, B.; Schlick, S. *J. Polym. Sci., Part B: Polym. Phys.* **2002**, *40*, 424.

(3) Bokria, J. G.; Schlick, S. *Polymer* **2002**, *43*, 3239.

(4) Pukansky, B. In *Polymeric Materials Encyclopedia*; Salamone, J. C., Ed.; CRC Press: Boca Raton, FL, 1996; pp 6615−6623.

(5) Albizzati, E.; Giannini, U.; Collina, G.; Noristi, L.; Resconi, L. In *Polypropylene Handbook*; Moore, E. P., Jr., Ed.; Hanser Publishers: Munich, 1996; Chapter 2, p 92.

(6) (a) Mirabella, F. M. *Polymer* **1993**, *34*, 1729. (b) Mirabella, F. M. *J. Polym. Sci., Part B: Polym. Phys.* **1994**, *32*, 1205. (c) Mirabella, F. M., Jr.; McFaddin, D. C. *Polymer* **1996**, *37*, 931.
(7) Xu, J.; Feng, L.; Yang, S.; Wu, Y.; Yang, Y.; Kong, X. *Polymer* **1997**, *38*, 4381.
(8) Feng, Y.; Hay, J. N. *Polymer* **1998**, *39*, 6723.
(9) Zhu, X.; Yan, D.; Fang, Y. *J. Phys. Chem. B* **2001**, *105*, 12461.
(10) Kamfjord, T.; Stori, A. *Polymer* **2001**, *42*, 2767.
(11) (a) Fan, Z. Q.; Zhang, Y.-Q.; Xu, J.-T.; Wang, H.-Tao.; Feng, L.-X. *Polymer* **2001**, *42*, 5559. (b) Xu, J.-T.; Fu, Z.-S.; Fan, Z. Q.; Feng, L.-X. *Eur. Polym. J.* **2002**, *38*, 1739.
(12) Varghese, B.; Kruczala, K.; Bokria, J. G.; Schlick, S. *Macromolecules* **2003**, *36*, 1899.
(13) Delprat, P.; Duteurtre, X.; Gardette, J.-L. *Polym. Degrad. Stab.* **1995**, *50*, 1.
(14) Gensler, R.; Plummer, C. J. G.; Kausch, H.-H.; Kramer, E.; Pauquet, J.-R.; Zweifel, H. *Polym. Degrad. Stab.* **2000**, *67*, 195.
(15) Stegge, J. M.; Urban, M. W. *Polymer* **2001**, *42*, 5479.
(16) Spalek, T.; Kruczala, K.; Schlick, S., manuscript in preparation.
(17) Lucarini, M.; Pedulli, G. F. *Makromol. Chem.* **1997**, *252*, 179 and references therein.
(18) (a) Goldberg, D. E. *Genetic Algorithms in Search, Optimization and Machine Learning;* Addison-Wesley: Reading, MA, 1989. (b) Michalewicz, Z. *Genetic Algorithms + Data Structures = Evolution Programs;* Springer-Verlag: Berlin, 1992.
(19) Hartke, B. *J. Chem. Phys.* **1993**, *97*, 9973.
(20) Niesse, J. A.; Mayne, H. R. *Chem. Phys. Lett.* **1996**, *261*, 576.
(21) Nikitas, P.; Papageorgiou, A. *Comput. Phys. Commun.* **2001**, *141*, 225.
(22) Maltempo, M. M.; Eaton, S. S.; Eaton, G. R. In *EPR Imaging and In Vivo EPR*; Eaton, S. S., Eaton, G. R., Ohno, K., Eds.; CRC Press: Boca Raton, FL, 1991; Chapter 14, p 145.
(23) Marek, A.; Schlick, S., unpublished work from this laboratory. See also refs 1c−e.
(24) Gillen, K. T.; Clough, R. L. *Polymer* **1992**, *33*, 4359.
(25) Malik, J.; Hrivik, A.; Tuan, D. Q. In *Polymer Durability: Degradation, Stabilization and Lifetime Prediction*; Clough, R. G., Billingham, N. C., Gillen, K. T., Eds.; Adv. Chem. Ser. 249; American Chemical Society: Washington, DC, 1996; Chapter 29, p 455.
(26) The diffusion coefficients, *D*, of nitroxides measured in PP are different compared to those measured for Tinuvin 770. The value of 2.55×10^{-9} cm^2 s^{-1} was deduced by ESRI in PP plaques at 333 K.[27] This result is in good agreement with the value of 1.49×10^{-9} cm^2 s^{-1} deduced at 353 K by a different method: A stack of PP sheets (100 μm thick) was pressed under vacuum and sandwiched between PP plaques containing an excess of HAS−NO; at the end of the experiment each sheet was peeled from the stack, and its nitroxide content was measured by ESR.[28] In the Discussion of this paper (vide supra), we have compared diffusion coefficients for Tinuvin 770 measured by the same method in PP and LDPE.[21]
(27) Franchi, P.; Lucarini, M.; Pedulli, G. F.; Bonora, M.; Vitali, M. *Macromol. Chem. Phys.* **2001**, *202*, 1246 and references therein.
(28) Dudler, V. *Polym. Degrad. Stab.* **1993**, *42*, 205.
(29) Rabello, M. S.; White, R. J. *Polymer* **1997**, *38*, 6379, 6389.
(30) Morris, H. R.; Monroe, B.; Ryntz, R. A.; Treado, P. J. *Langmuir* **1998**, *14*, 2426 and references therein.
(31) Pennington, B. D.; Ryntz, R. A.; Urban, M. W. *Polymer* **1999**, *40*, 4795.
(32) Fitchmun, D. R.; Mencik, Z. *J. Polym. Sci., Polym. Phys. Ed.* **1973**, *11*, 951.

MA025701Q